ELSEVIER

Nuclear Instruments and Methods in Physics Research A 356 (1995) 189–195

NUCLEAR INSTRUMENTS & METHODS IN PHYSICS RESEARCH Section A

Influence of external grounded screens on the electric field structure in a drift chamber

G.E. Gavrilov [a,*], A.G. Krivshych [a], M.K. Jarmarkin [b]

[a] *High Energy Physics Division, Petersburg Nuclear Physics Institute, PNPI, Gatchina, St.-Petersburg 188350, Russian Federation*

[b] *St.-Petersburg State Technical University, St.-Petersburg, Russian Federation*

Received 7 January 1994; revised form received 26 August 1994

Abstract

The structure of electric fields in a drift chamber is considered both taking into account the influence of adjacent components and the presence of dielectric walls. It is shown that additional field shaping electrodes can preserve the uniformity of the electric field in the detector and protect it from the distortion by an external grounded screen. This design allows the first drift cell to end as close as 5 mm from the outer surface of the grounded screen. It was incorporated in the FTC detector in the L3 experiment at CERN.

1. Introduction

The present work has been done during the design of the end cap detector FTC (forward tracking chamber) for the L3 experiment at LEP. The FTC consists of two layers of modules, each of which contains four drift cells. Modules in the layer are oriented at 90° with respect to those in the other to provide an orthogonal coordinate system. However, each drift cell provides both coordinates via drift time and charge division. The electric field structure in the module was designed to achieve the required space resolution of $\sigma \leq 150$ μm and an angle resolution better than 10 mrad in the range of polar angle $8° \leq \theta \leq 35°$. The space for the FTC was severely limited to the narrow gap ($\Delta Z \simeq 70$ mm) between the central detector (TEC) and electromagnetic calorimeter (BGO) – see Fig. 1. These required reliable electrical shielding from the disturbing effects of the neighboring detectors. It should be noted that the charge division method is especially sensitive to such influences. Hence, these space limitations make the required performance difficult to achieve. As a consequence of the space limitation, the strips of the field shaping electrodes were placed only 2 mm from the detector drift cell. This required very precise determination of the potentials on the strips. For the same reason, the external grounded screens can not be further than 2 mm from the surface of detector. As was shown in Ref. [1], in such a situation the electric field in the outer drift cells is distorted and the relationship between drift time and position becomes nonlinear especially for the outer drift cells. Also the gas gain is different for different cells which degrades the space resolution of the detector. Such problems existed in various detectors [2–4]. However, in those cases, there was enough space to minimize edges effects by locating the grounded screens sufficiently far away.

2. Construction of the FTC detector

As mentioned above, the FTC end cap consists of the two 1 m diameter layers of drift modules (Fig. 2). Each module contains in the median plane four signal wires (SW) between field shaping wires (FW). The distance between adjacent wires are 3 mm, with only 2 mm between the edge FW and the chamber wall. Two drift spaces of 22 mm are symmetric with respect to the wire plane and contained by 0.5 mm thick copper-clad fiberglass cathodes. The side walls are 1.5 mm thick fiberglass plates with printed field shaping strips on the inner side, 0.5 mm wide on a 2 mm period. These provide a uniform electric field with equipotential planes parallel to the median plane. The precise high voltage divider based on thick film technology was designed and produced specially for FTC. The temperature stability of the divider is 5×10^{-4} per degree and the resistors variation was not worse than 1×10^{-3}. The cathodes, strips and FW are connected to negative high voltage and the SW are kept at ground potential.

* Corresponding author. Tel. +7 812 294 91 43, fax +7 812 298 02 57, e-mail hepdivis@lnpi.spb.su.

0168-9002/95/$09.50
SSDI 0168-9002(94)01321-7

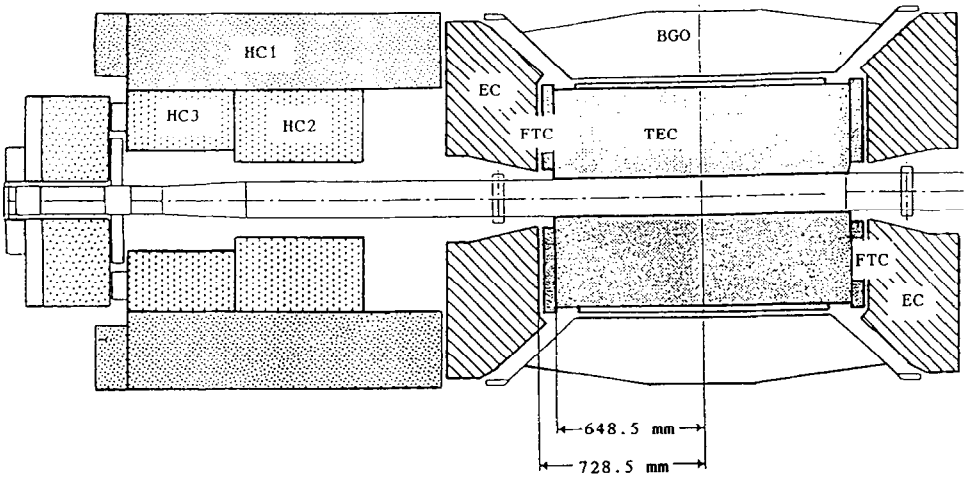

Fig. 1. Cross section view of L3 end caps. HC1, HC2, HC3 – hadron calorimeter. EC-BGO electromagnetic detectors end caps. TEC – central time expansion chamber. FTC – forward/backward tracking chamber.

3. Mathematical model for the computation of the potentials and field distribution in an FTC

The method of integral equations was used to calculate electrical field in FTC. This method is presented in Appendix A. It was considered a two-dimensional task, and charges both in the detector volume and on the dielectric surface were neglected. The real dimensions of the field shaping electrodes, wires and the presence of dielectric walls were taken into account. The computation was carried out in a quoter module due to the symmetry of the field structure. The maximum calculations error was estimated to be not above $\pm 0.5\%$ in considered region. We did not use the standard program package GARFIELD for our calculation as one cannot provide the real geometry of FTC in presence of the grounded screens and dielectric walls [5].

4. Results of calculations

4.1. The structure of the electric field in the drift chamber without external grounded screen

Fig. 3 presents the field in a FTC module with only the internal field-shaping strips. To calculate the potentials of strips the initial assumption was made that the wire plane consists of an infinite series of grounded SWs alternated with thicker FWs at a potential U_F. Then at the second stage of calculation it happened that introducing the physical realization of the strips on a dielectric wall with $\varepsilon = 5$ did not significantly change the ideal field structure in the active region of the drift cells. In Fig. 4 the distribution of the longitudinal component of the field intensity $E_y(Y)$ along the side boundary ($X = 6$ and 12 mm) near an outer signal wire (SW) is shown. It is seen that starting from $Y \simeq 7$ mm along the boundary of the drift space ($X = 12$ mm) the electrical field becomes almost uniform $|\Delta E/E| \leq 2\%$ and exceeds the requirement for space resolution. In this situation we have got a good coincidence with GARFIELD simulation, too (Fig. 4).

The granularity of the strips has a negligible effect on the field at a distance $\Delta X = 2$ mm from the side wall of module (Fig. 5).

4.2. The influence of the external grounded screen

To ensure the reliable protection of the chamber against electromagnetic noise of external devices, two grounded screens were installed on both sides of the end cap detector. The distance between the inner field-shaping strips of FTC and the closest screen is 3.5 mm. The intense electric

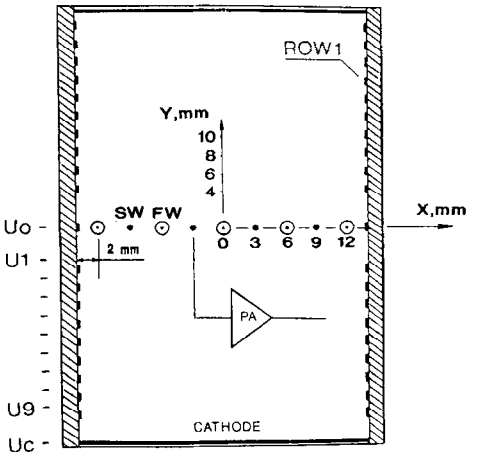

Fig. 2. Schematic view of jet type drift module which contains in the median plane four signal wires (SW) between field shaping wires (FW).

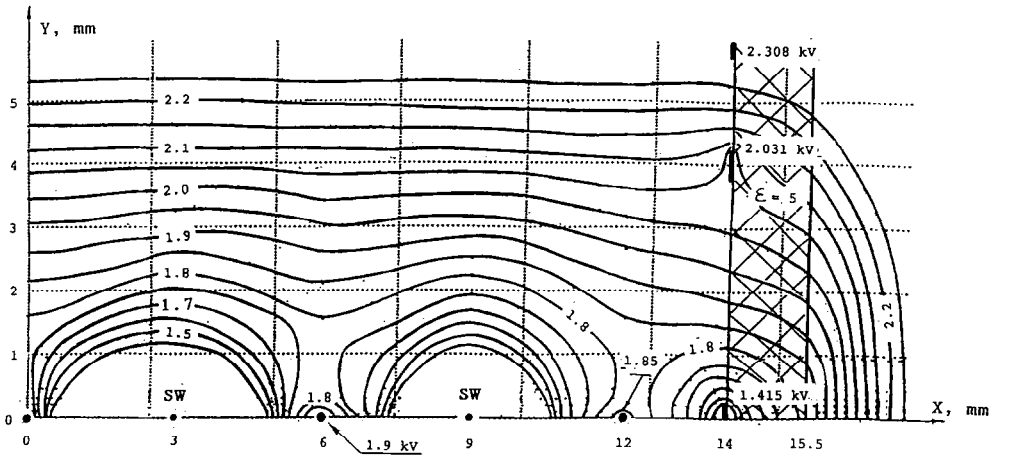

Fig. 3. Computer simulation of the electric field in FTC module with only the internal field shaping strips – ROW 1.

field between the field shaping strips and adjacent screen causes the equipotential lines to be deflected away from the wire plane as they approach the strips inside the chamber. This intense field penetrates the gaps between the strips and distorts the field inside the module (Fig. 6). Fig. 7 shows the same variables as Fig. 4 except in the presence of the shielding screen. It is seen that the uniform field region is destroyed even near the center in the range Y = 7–22 mm, $E_y(Y)$ changes from 0.139 kV/mm up to 0.16 kV/mm or 15%! The distortion is worse in the outer cells. One can see that the effects of the strip granularity are much more apparent. Figs. 8 and 9 compare the dependence of $E_y(Y)$ close to the strips with and without an external screen. It is clear that the presence of the screen strongly changes the field structure between the strips closest to the wire plane, increasing the field intensity on the edges of the first strip by a factor of five reaching E_y = 1.5 kV/mm. That is inadmissible because it would provoke sparking on the edges of strips.

4.3. *Method of electrostatic protection of the drift chamber*

In order to prevent the grounded screen from distorting the internal field, we placed an additional plane of strips (ROW2) between the screen and the original strips. The additional row of strips have the same period and potential distribution but is staggered with respect to the inside row (Fig. 10). The resistor chain remains unchanged. In this case all the field distortions are localized in the gap between the outer strips and the screen. The gap between the two rows of strips is a protective buffer and protects the drift space from the penetration of distorting fields. We calculated the field structure for three arrangements of additional strips. In the first case strips are opposite one to another. In the second and third, the rows are displaced above and below by 1 mm. It turned out that all three geometries provide adequate uniformity of the electrical field in spite off of the existence of the external screen. However a comparative analysis shows that it is preferable to place each strip 1 mm

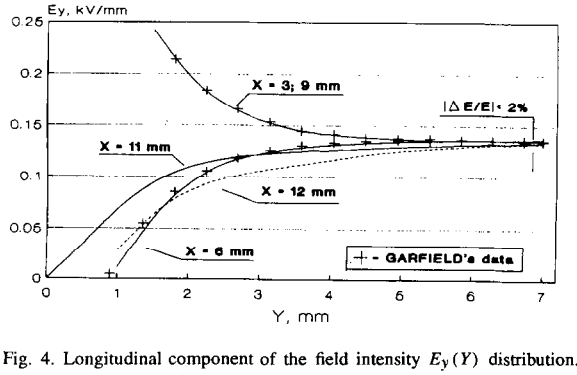

Fig. 4. Longitudinal component of the field intensity $E_y(Y)$ distribution. X = 6 mm and X = 12 mm – boundaries of the margin drift cell. X = 3 mm and X = 9 mm – coordinates of the inner and outer signal wires. X = 11 mm – coordinate of the mid point in the drift cell.

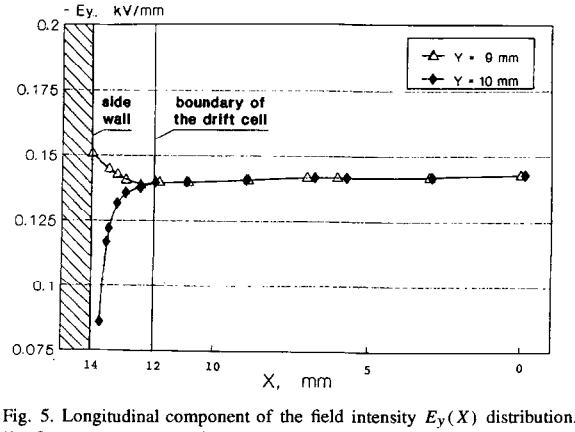

Fig. 5. Longitudinal component of the field intensity $E_y(X)$ distribution. Y = 9 mm – coordinate of the mid point between strips. Y = 10 mm – the center of the strip.

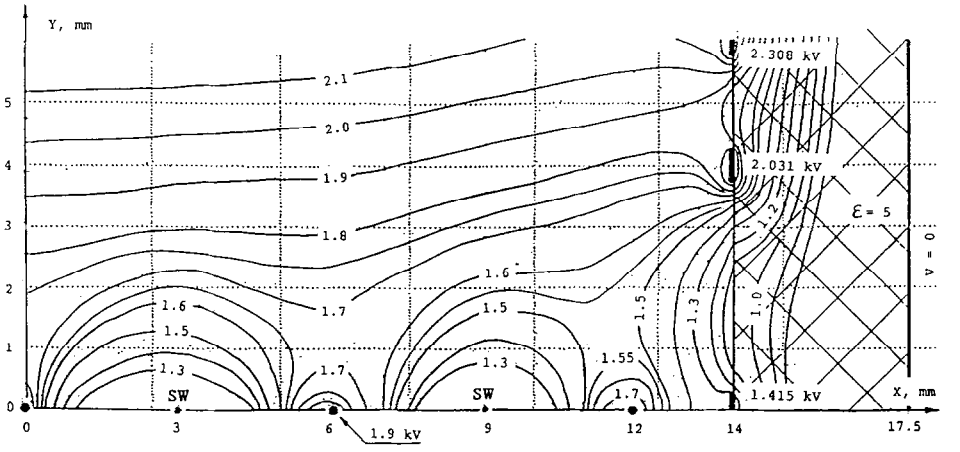

Fig. 6. Computer simulation of the electric field in FTC module surrounded by the grounded screens.

below the inner one at the same potential.

Fig. 11 shows the longitudinal $E_y(Y)$ and tangential $E_x(Y)$ components of field for three values of X corresponding to 0.1, 0.5, and 2.0 mm from the inner strips. It is clear that starting from the boundary of the outer drift cell (X = 12 mm), the longitudinal component is constant at E_y = 0.14 kV/mm and unaffected by the strips granularity. Equipotential lines become parallel to the anode plane and E_x becomes small inside of this line.

Fig. 12 shows the same components but between the two layers of strips, in the dielectric of the side wall. Comparison of Figs. 14 and 15 shows that the proposed method not only permits favorable redistribution of the external field but also limits electrical intensity values between inner and outer strips rows. As a result the field intensity on the edges of the strips is E_y = 0.4 kV/mm (Fig. 11, X = 13.9 mm) instead of E_y = 1.5 kV/mm in Fig. 9. This practically eliminates any risk of sparking on the inner strips of FTC. On the edges of the outside strips the field intensity increases up to E_y = 1.0 kV/mm (Fig. 12, X = 15.5 mm). However, this plane of strips is easy to passivate by painting of varnish, providing reliable operation of the detector. The distribution of the equipotential lines close to the anode plane is presented in Fig. 13. In Figs. 14 and 15 the dependence of the longitudinal $E_y(Y)$ and tangential components $E_x(Y)$ over the total range of coordinates is shown. It is seen that the entire active volume of the FTC ($|X| \leq 12$ mm and $5 \leq Y \leq 22$ mm) the field is uniform within 0.5%. It may be noted that the field structure near the signal wires becomes insensitive to the influence of the external screen.

To illustrate the efficiency of the proposed method the ratio of pulse heights produced by 5.9 keV X-rays from a ^{55}Fe source is shown (Fig. 16), when the grounded screen is located in L = 2 mm from the module. It is seen that the electrostatic protection makes negligible (about 1%) the influence of the grounded screen on the ratio of SWs pulse heights [6].

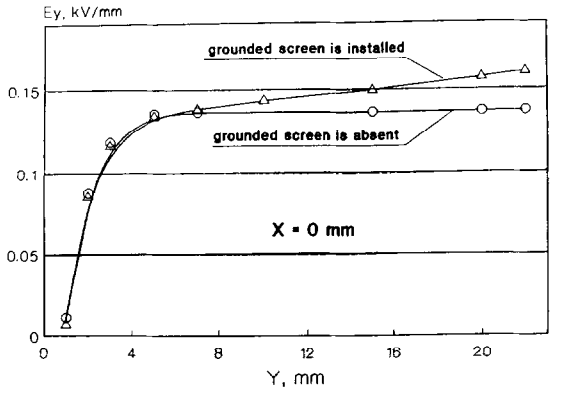

Fig. 7. Longitudinal component of the field intensity $E_y(Y)$ distribution. X = 0 mm - middle of the drift module.

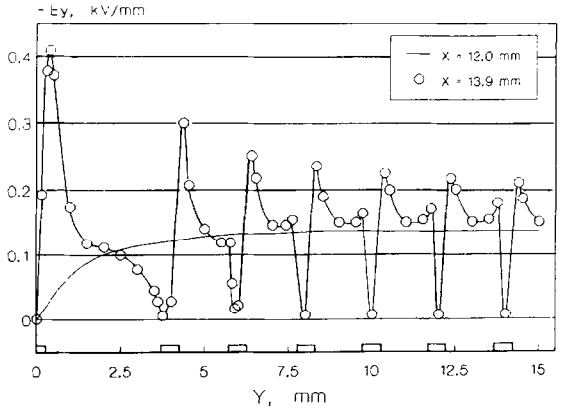

Fig. 8. Distribution of the $E_y(Y)$ without an external grounded screen. X = 12 mm - boundary of the margin drift cell. X = 13.9 mm - coordinate near by the surface of the side wall.

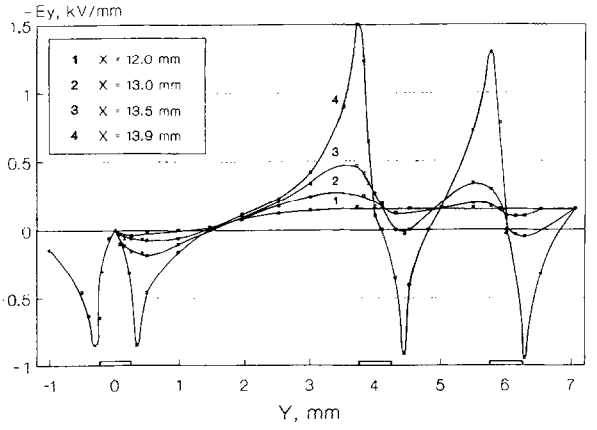

Fig. 9. Distribution of the $E_y(Y)$ in presence of the grounded screen.

5. Conclusion

It has been shown that the proposed method of electrostatic protection of the detector provides the required uniformity of field and does not permit intrusion by the external field. The field shaping electrode structure is compact (3.5 mm between inner strips and screen) and may be placed as close as 2 mm from the active region of the edge signal wires. The chosen strip arrangement results in moderate surface fields on the strip edges, and hence stable operation.

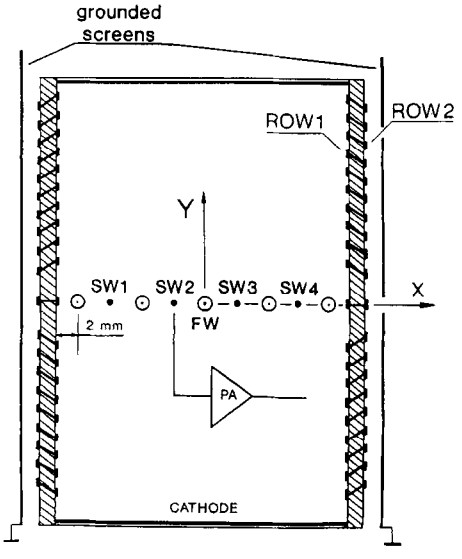

Fig. 10. Schematic view of FTC drift module with an additional plane of strips (ROW2).

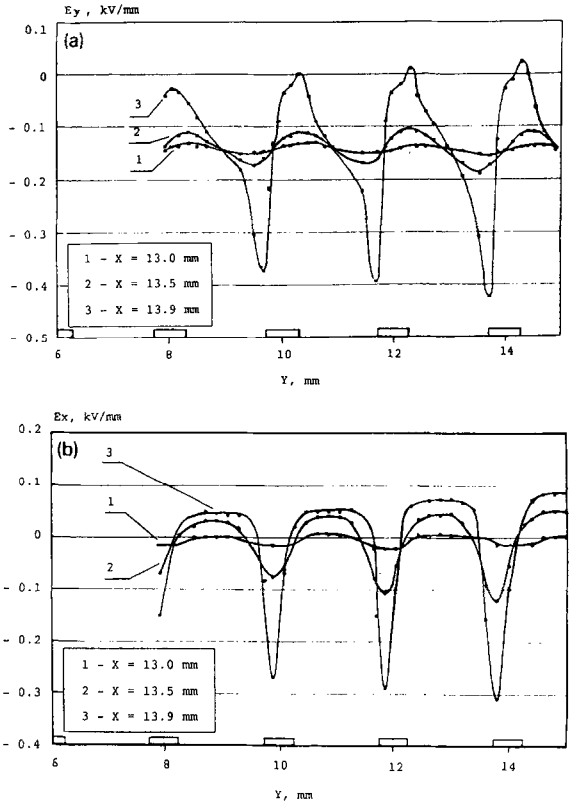

Fig. 11. (a) Longitudinal $E_y(Y)$ and (b) tangential $E_x(Y)$ components of the electric field for values of X distant on 0.1 mm, 0.5 mm and 1.0 mm from the inner strips.

Acknowledgement

It is a pleasure to thank A. Miller (TRIUMF) for his tolerance and kind interest in discussing the present work. The authors are indebted to R. Veenhof and V.A. Andreev for encouragement and criticism. We would like to thank V.M. Kuzmin for his efforts in the shaping of the draft.

Appendix A

To calculate the electric field structure in FTC modules the method of Fredholm integral equations was used. Let's consider the system of m charged bodies. Then the line $L_m(x, y)$ in the two-dimensional coordinate system (x, y) limits the outlines of the mth body ($m = 1, 2, \ldots, M$). In this case the potential formed in the point of space by the outline element dl may be written as:

$$d\varphi = \frac{\sigma_m\, dl}{2\pi\varepsilon} \ln\left(\frac{1}{r(x,y)}\right),$$

where σ_m is the surface charge density of the dl element; r is the distance from the space point to dl. The potential formed by all charged bodies is:

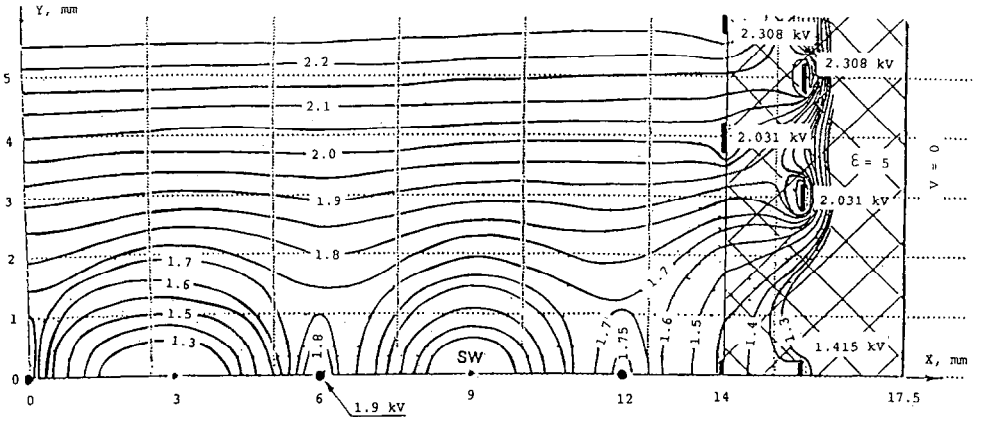

Fig. 13. Distribution of the equipotential lines close to the anode plane in FTC module with two rows of the strips.

$$\varphi = \sum_{m=1}^{M} \int_{L_m} \frac{\sigma_m \, \mathrm{d}l}{2\pi\varepsilon} \ln\left(\frac{1}{r(x,y)}\right) \mathrm{d}l\,, \qquad \text{(A.1)}$$

where the integration is done along the outlines of the mth body L_m and summation index runs over the all charged bodies. For this calculation the outline L_m was divided into several pieces, and a linear-spline approximation of the unknown function $\sigma_m(x,y)$ was used:

$$\sigma_{mj}(x,y) = a_{mj} l + b_{mj}\,, \qquad \text{(A.2)}$$

with

$$l_{mj} \le l \le l_{m,j+1}\,,$$

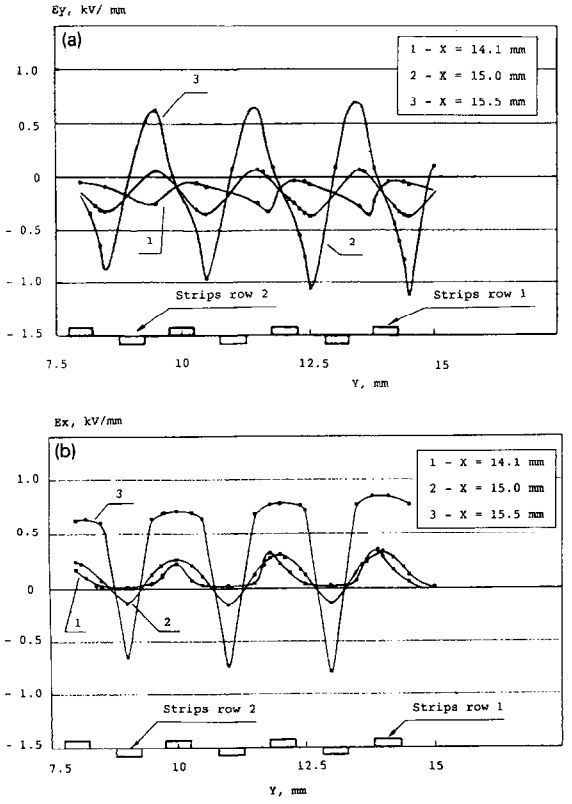

Fig. 12. (a) Longitudinal $E_y(Y)$ and (b) tangential $E_x(Y)$ components of the electric field for values of X between the two layers of strips.

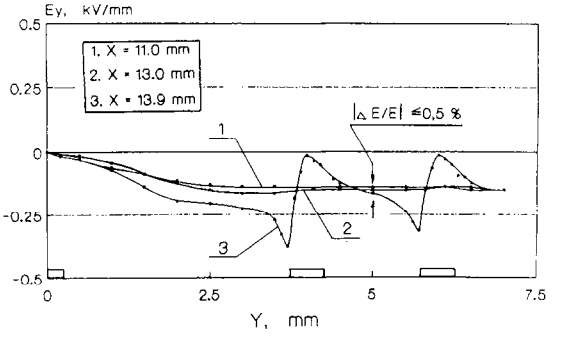

Fig. 14. Dependencies of the longitudinal $E_y(Y)$ and tangential components $E_x(Y)$ over the range of X = 11–13.9 mm.

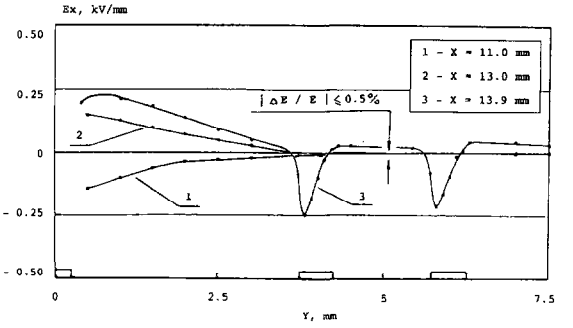

Fig. 15. Dependence of the tangential $E_x(Y)$ component over the range of X = 11–13.9 mm.

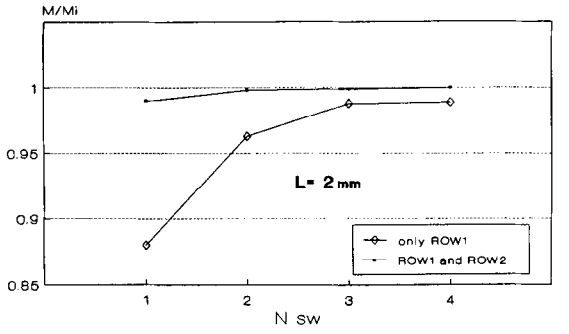

Fig. 16. Influence of the grounded screen on the ratio of pulse heights produced by 5.9 keV X-rays from a ^{55}Fe source both in absence (only ROW1) and in presence (ROW1 and ROW2) of the electrostatic protection. Were M is the pulse height of signal wire when the grounded screen is in a distance L = 2 mm from the module and M_i is the pulse height without the grounded screen.

where l_{mj} is a fixed point on the outline and a_{mj} and b_{mj} are equal to:

$$a_{mj} = \frac{\sigma_{mj+1} - \sigma_{mj}}{l_{mj+1} - l_{mj}}, \tag{A.3}$$

$$b_{mj} = \frac{\sigma_{mj} l_{mj+1} - \sigma_{mj+1} l_{mj}}{l_{mj+1} - l_{mj}}. \tag{A.4}$$

Writing a boundary condition of the first kind to the ξ_i points we got the system of the linear algebraic equations with respect of the unknown σ_j:

$$\varphi(\xi_i) = \sum_{m=1}^{M} \sum_{j=1}^{J_m} \sigma_{mj} A_{mj}, \tag{A.5}$$

when the points ξ_i are chosen on the surfaces of the bodies with a given potential. The coefficients A_{mj} are found by substitution Eqs. (A.2) and (A.3), (A.4) in Eq. (A.1) and integration along L_m. To write the boundary conditions of the second kind for the points on the boundary with materials with a different dielectrical constant we used the equation:

$$\sigma_j = \frac{\lambda}{\pi} \sum_{m=1}^{M} \int \frac{\sigma_m \cos(\boldsymbol{r}_m, \boldsymbol{n}_m)}{r(x,y)} \, \mathrm{d}l, \tag{A.6}$$

with

$$\lambda = \frac{\varepsilon_1 - \varepsilon_2}{\varepsilon_1 + \varepsilon_2},$$

where ε_1 and ε_2 are the dielectrical constants for two materials, $\boldsymbol{n}_m$ is a vector normal to the boundary directed towards the material with dielectric constant ε_1, and $\boldsymbol{r}_m$ is the vector connecting the point ξ_i with the a point of the surface.

Substitution of the Eqs. (A.2) and (A.3), (A.4) in Eq. (A.6), permits to complete the system (A.5) with the following boundary conditions:

$$\sum_{m=1}^{M} \sum_{j=1}^{J_m} \sigma_{mj} B_{mj} = 0. \tag{A.7}$$

The joint solution of the Eqs. (A.5) and (A.7) permits to determine the charge densities. Then to determine the potential in the drift space, Eq. (A.1) was used. The components of the electric field strength were determined by values the derivatives of Eq. (A.1) with respect to the coordinates:

$$E_x = \frac{\partial \varphi(x,y)}{\partial x} = -\sum_{m=1}^{M} \int_L \frac{\sigma_m}{2\pi\varepsilon} \frac{\partial}{\partial x} \ln\left(\frac{1}{r(x,y)}\right) \mathrm{d}l,$$

$$E_y = \frac{\partial \varphi(x,y)}{\partial x} = -\sum_{m=1}^{M} \int_L \frac{\sigma_m}{2\pi\varepsilon} \frac{\partial}{\partial y} \ln\left(\frac{1}{r(x,y)}\right) \mathrm{d}l. \tag{A.8}$$

The calculation of the electric field structure in the drift space was carried out keeping in mind the plane parallel character of the field distribution in the middle. We also took advantage of the symmetry in the $x = 0$ and $y = 0$ planes.

References

[1] A. Weltin, Nucl. Instr. and Meth. A 264 (1988) 213.
[2] E. Barrelet et al., Nucl. Instr. and Meth. 200 (1982) 219.
[3] M. Atac et al., Nucl. Instr. and Meth. A 269 (1988) 40.
[4] H. Anderhub et al., Nucl. Instr. and Meth. A 252 (1986) 357.
[5] R. Veenhof, GARFIELD manual (v.4.18) CERN (1993).
[6] V. Andreev et.al., Preprint 1797, Gatchina (1992).